Fermi National Accelerator Laboratory

FERMILAB-Conf-90/40

Nonlinear Plasma and Beam Physics in Plasma Wake-Fields*

J. B. Rosenzweig

Fermi National Accelerator Laboratory
P.O. Box 500
Batavia, Illinois 60510

February 12, 1990

* Submitted to the proceedings of the LaJolla Topical Conference on Research Trends in Nonlinear and Relativistic Effects in Plasmas, LaJolla, California, February 5-8, 1990.

February 12, 1990

NONLINEAR PLASMA AND BEAM PHYSICS IN PLASMA WAKE-FIELDS

J. B. ROSENZWEIG[†]

Fermi National Accelerator Laboratory
P.O. Box 500, M.S. 306,
Batavia, Illinois 60510

ABSTRACT

In experimental studies of the Plasma Wake-field Accelerator performed to date at the Argonne Advanced Accelerator Test Facility, significant nonlinearities in both plasma and beam behavior have been observed. The plasma waves driven in the wake of the intense driving beam in these experiments exhibit three-dimensional nonlinear behavior which has as yet no quantitative theoretical explanation. This nonlinearity is due in part to the self-pinching of the driving beam in the plasma, as the the denser self-focused beam can excite larger amplitude plasma waves. The self-pinching is a process with interesting nonlinear aspects: the initial evolution of the beam envelope and the subsequent approach to Bennett equilibrium through phase mixing.

Submitted to the Proceedings of the LaJolla Topical Conference on Research Trends in Nonlinear and Relativistic Effects in Plasmas, LaJolla, California, Feb. 5–8, 1990.

[†]Also at Argonne National Laboratory, Argonne, IL 60439.

1. Introduction

The Plasma Wake-field Accelerator,[1-4] (PWFA), a scheme in which charged particles are accelerated in the potentially ultra-high gradient fields supported by plasma waves driven in the wake of an intense particle beam, has been the subject of experimental investigation at the Argonne Advanced Accelerator Test Facility[5,6] (AATF). In course of these experiments, many aspects of nonlinear plasma and beam physics have been observed. These include the driving of nonlinear plasma waves in the wake of the beam, and the behavior of the beam itself under the influence of its strong, nonlinear self-focusing wake-fields. This self-focusing effect yields considerably larger lens strengths than conventional methods, a fact which has led to the proposal of employing plasma wake-fields to create a powerful final focusing lens for use in a future linear e^+e^- collider.[7-11] The first compelling evidence for electron beam self-focusing in the PWFA tests at the AATF was in fact the observation of nonsinusoidal plasma wave supported wake-fields left behind the driving beam. At high driving beam currents the accelerating wake-fields were enhanced in both amplitude and in harmonic content beyond what was expected assuming the driving beam did not pinch. The degree of nonlinearity in the wake-fields provided an estimate on the self-pinched driving beam radius; this estimate agreed well with what was calculated from the theory of plasma focusing.[6]

The experimentally observed nonlinear plasma waves represent one aspect of nonlinear physics, the deviation from linear dynamics with increasing amplitude. The theoretical problem of describing nonlinear electron plasma waves excited by relativistic electron beams has been examined thoroughly the in one-dimensional limit.[12-17] On the other hand, due to the mathematical difficulty of the analysis, not much progress has been made in treating three-dimensional nonlinear plasma waves. Theoretical estimates of the expected degree of wake-field wave nonlinearity in the experiments at the AATF were based on a rough synthesis of three-dimensional linear[7] and one-dimensional nonlinear PWFA theories. This

estimation method and its limitations are outlined below, and the results of this analysis are compared with the experimental data. The present status of and future prospects for theoretical work on the three-dimensional theory of nonlinear plasma waves are examined.

After the discussion of nonlinear plasma waves in PWFA research, the investigation of nonlinear dynamics in the self-pinching electron beam will be undertaken in detail. The nonlinear physics contained in the driving beam dynamics has some similarity to the nonlinear plasma waves in that the nonsinusoidal envelope motion results in a steep density spike, although this motion rapidly dissipates. Even ideal envelope wave motion requires an intrinsically nonzero transverse beam temperature, in contrast to the essentially cold fluid behavior of the nonlinear wake plasma waves. The combined effects of the beam temperature and the nonlinearity of the self-focusing forces cause the coherent envelope motion to be collisionlessly damped to approach an equilibrium through the mechanism of fast phase mixing. This equilibrium corresponds to a Bennett density profile whose minimum width is determined by the beam current and initial temperature.

The beam dynamics is treated both analytically and computationally. Because in a certain limit the focusing wake-fields become nearly independent of the plasma density and depend only on the beam profile, the self-consistent evolution of the beam distribution can be treated as an issue approximately separate from the plasma dynamics. Analytical models of the self-pinch process are employed below: laminar flow is assumed in calculating the initial focusing dynamics, and the Maxwell-Vlasov equation is utilized to discuss the asymptotic approach to self-pinched equilibrium. Particle-in-cell computer simulations are shown to complement and clarify the conclusions of the analysis, and to examine the collisionless approach to equilibrium more completely. The physics of the self-pinched beam is then compared to the related process of emittance growth of a space charge dominated beam in a linear focusing channel. After the theoretical context is established, results from the AATF experimental measurements

are presented and compared with the theory.

2. Linear Plasma Wake-field Theory

In the linear theory of plasma wake-fields the function of the bunched beam is to provide an impulse to the plasma electron fluid, which causes electron density oscillations to be excited at the plasma frequency $\omega_p = \sqrt{4\pi e^2 n_0/m_e}$, where n_0 is the equilibrium ambient electron density. Linearization of the fluid equations requires that the perturbed electron density $n_1 \equiv n - n_0$ be a small quantity compared to n_0. The linearized fluid equation for plasma oscillations excited by an electron beam is given by

$$\frac{\partial^2 n_1}{\partial t^2} + \omega_p^2(n_1 + n_b) = 0, \tag{2.1}$$

where n_b is the beam density. If one assumes a steady state condition where the plasma response in time t and longitudinal coordinate z is given only in the combination $\xi = z - v_b t$, with the beam velocity $v_b = \beta_b c$ taken to be constant (in practice we are concerned almost entirely with ultra-relativistic beams with $v_b \simeq c$), then Eq. (2.1) can be written as

$$\frac{\partial^2 n_1}{\partial \xi^2} + k_p^2(n_1 + n_b) = 0, \tag{2.2}$$

where $k_p = \omega_p/v_b$. This linear model of plasma oscillations yields a picture of independent local oscillators with natural frequency ω_p excited by a source moving with velocity v_b, giving rise to a simple dispersionless wave with phase velocity $v_\phi = v_b$.

If we can write the driving beam density for a cylindrically symmetric beam as a product of longitudinal and transverse distributions, $n_b = g(\xi)f(r)$, with g

normalized to unity, then the solution to Eq. (2.2) can is

$$n_1(\xi, r) = f(r) \int_{\xi}^{\infty} d(k_p \xi') g(\xi') \sin [k_p(\xi - \xi')]. \tag{2.3}$$

The radial profile of the plasma wave amplitude is the same as that of the beam; a convolution integral over beam's current profile gives the the longitudinal response. This convolution over the beam pulse gives a maximum excited wave if the beam scale length is shorter than a plasma skin-depth k_p^{-1}, approaching $\|n_1(r)\| = k_p f(r)$. If the beam has a Gaussian current profile, then evaluation ot the convolution integral gives the degradation of the wave amplitude with rms beam length σ_z explicitly; $\|n_1(r)\| = k_p f(r) \exp [-(k_p \sigma_z)^2/2]$.

Notice that in the limit that the beam bunch is much wider than it is long the quantity $f(r)$ can be interpreted as a surface charge density. If the beam is also much wider than the plasma skin-depth, then the electric field can be easily approximated as arising from a one-dimensional charge distribution –

$$E_z \simeq 4\pi e \int_{\xi}^{\infty} [n_b(\xi') + n_1(\xi')] d\xi' \simeq 4\pi e f(r) \cos (k_p \xi). \tag{2.4}$$

Inclusion of the effects of the wave's finite transverse geometry requires substitution a function $F(k_p r)$ (which is a convolution over the transverse profile using the radial Green's function[7]) for $f(r)$ in Eq. (2.4). This function which is nearly proportional to $f(r)$ if the beam is wide compared to k_p^{-1}. In the opposite limit, the longitudinal field becomes logarithmically small and nearly constant inside the beam profile if the beam is narrow with respect to k_p^{-1}. This is due to the fact that the plasma motion, and the related electric field, becomes predominantly radial in this limit. To quantify this effect, we define the radial field efficiency $\eta_r(k_p \sigma_r)$ of the wave, which is the ratio of the convolution integral on axis $F(0)$ to its value in the limit that $k_p \to \infty$. The dependence of the on-axis longitudinal field on the width of the beam distribution σ_r is explicit in this definition.

The efficiency $\eta_r(k_p\sigma_r)$ is a monotonically increasing function of its argument, approaching unity at large values of $k_p\sigma_r$.

The most relevant remaining facet of the linear theory concerns the strong transverse wake-fields which act upon the beam itself. In general, if the longitudinal/temporal dependence of the plasma response can be expressed as a function of ξ alone, as we have assumed, then the wake-field in the limit of an ultra-relativistic beam

$$\mathbf{W} \equiv \mathbf{E} + \hat{\boldsymbol{z}} \times \mathbf{B} \tag{2.5}$$

can be derived from a potential,

$$\mathbf{W} = \nabla(A_z - \phi) \tag{2.6}$$

This is a differential form of the Panofsky-Wenzel theorem,[18] which will explicitly manifest itself in the nonlinear wake-field data we will discuss below. In the wake plasma wave, the longitudinal component of the electromagnetic vector potential A_z vanishes and the wave is electrostatic. Inside the beam itself, however, A_z does not vanish in general, and can give rise to magnetic self-pinching forces.

The most interesting regimes occur in the limit that the beam is long compared to the plasma skin-depth, in which case the beam can be nearly charge neutralized, *i.e.* $n_1 = -g(\xi)f(r)$. If in addition the beam is wide compared to the skin-depth, then the plasma electron return current will flow inside of the beam, and the net force on the beam is approximately nullified, as the beam charge and current densities are neutralized. In such a case, charged particles moving in the direction opposite to the beam also feel no net force. This scheme, called plasma compensation, has been proposed as a method of alleviating problems associated with the strong beam-beam interaction in high energy linear colliders.[19]

In practice, high energy electron beams tend to be long and narrow, thus allowing choice of plasma density which gives a skin-depth small compared to the beam length, but large compared to its width. In this case, the plasma

return current flows in a disk of radius $\sim k_p^{-1}$ and the beam current density is not neutralized. The net force felt by the beam particles is thus the self-focusing effect of the magnetic fields arising from the beam current distribution. Since the beam is assumed to be ultra-relativistic, this force can be estimated simply from Gauss' law,

$$F_r = -\frac{4\pi e^2 g(\xi)}{r} \int_0^r r' f(r') dr'. \tag{2.7}$$

In this approximation the force depends only on the enclosed current density at a given point (r, ξ). Since the current density is not uniform inside the beam in general, the self-focusing wake-fields are not linear in r and independent of ξ as one would desire for aberration-free optics. The effects of the focusing nonlinearities on the performance of a plasma lens used near the interaction point of a linear collider has been examined extensively in Refs. 8-11.

From the discussion above, it would seem that there are two distinct regimes where the plasma wake-fields can provide large fields which may be of use in accelerator physics. If one utilizes an appropriate density plasma the short, wide beam can be used to drive large amplitude waves with high-gradient electric fields useful for accelerating other particle bunches, as in the PWFA. On the other hand, the long, narrow beam can be strongly focused by its self-magnetic fields which are left unbalanced when the plasma response neutralizes the beam's space charge density. It is in fact at the border of these two regimes that the most interesting experimental situation has been encountered, as will be seen below.

3. Nonlinear Plasma Wake-field Theory

The nonlinear theory of plasma wake-fields has not been developed to the point that the linear theory has, with the facility for calculating multi-dimensional effects. For this reason the theory is of limited practical use in quantitatively predicting or understanding experimental results. The one-dimensional treatments have, however, examined several relevant aspects of the nonlinear regime of the PWFA: modulational, convective and relativistic effects on the plasma waves,[13] improved transformer ratio (the ratio of the maximum accelerating field in the wake to the maximum decelerating field inside the driving beam) in the PWFA,[12] thermal limits on wave amplitude (wave breaking),[14],[15] and ion motion.[17] Despite the limitations of the theory, it is of instructive value to review the major results of the nonlinear treatments at this point.

The first nonlinear corrections to the linear theory arise through the effects of the convective derivative and the modulation of the bulk plasma electron density in the fluid equations. The nonrelativistic theory developed for this case entails keeping the full nonlinear terms in the fluid equation of motion, excluding the relativistically correct expression for the momentum. In this one-dimensional model the wave characteristics are dependent only on ξ. A useful form of the solution to nonrelativistic nonlinear fluid equation is in terms of harmonics of the plasma frequency, suppressing phase factors,[20]

$$n - n_0 = \sum_{m=1}^{\infty} \frac{m^m e^{ik\xi}}{2^{m-1} m!} \left(\frac{n_1}{n_0}\right)^m. \tag{3.1}$$

The quantity n_1 in this expression now represents the amplitude of the fundamental component of the plasma wave. The longitudinal electric field associated with this charge distribution is thus

$$E = 4\pi e k_p n_0 \sum_{m=1}^{\infty} \frac{m^{m-1} e^{ik\xi}}{2^{m-1} m!} \left(\frac{n_1}{n_0}\right)^m, \tag{3.2}$$

again ignoring phase factors. Note that if $n_1 = n_0$ in this expression that the elec-

tric field associated with the fundamental is $E = m_e c\omega_p/e$, which is referred to, somewhat inaccurately, as the "wave-breaking" field.[21] This harmonic decomposition of the electric field can be used to estimate the amplitude of the nonlinear waves in experiments if the harmonics in the longitudinal field are known. To incorporate the beam's role in the plasma wave excitation and the finite transverse dimension of the excited wave we add a factor to account for the radial efficiency

$$E = 4\pi e k_p n_0 \sum_{m=1}^{\infty} \frac{m^{m-1} e^{ik\xi} \eta_r(m k_p \sigma_r)}{2^{m-1} m!} (\frac{n_1}{n_0})^m, \tag{3.3}$$

and we equate our present definition n_1 with our previous usage, taking the amplitude of the fundamental to be that given by the linear theory, which for a cylindrically symmetric bi-Gaussian beam profile is

$$n_1 = \frac{k_p N \exp[-(k_p\sigma_z)^2/2]}{2\pi\sigma_r^2}, \tag{3.4}$$

where N is the number of particles per bunch, and $\sigma_{r(z)}$ is the rms beam radius (length).

The plasma waves that develop in the nonlinear nonrelativistic theory show steepening and an increasingly narrow spike in positive electron density as the amplitude is increased. This steepening, which is illustrated in Fig. 1, generates the harmonics which are contained in Eq. (3.1).

The addition of relativistic effects into the fluid treatment introduces an additional feature to the wave dynamics, that of period lengthening with increased amplitude. This phenomenon is shown for a moderately relativistic case in comparison to the nonrelativistic solution for the same maximum fluid electron velocity $v = \beta c$ in Fig. 1. The equation for one-dimensional plasma oscillations in the limit $v_b \to c$ with functional dependence only on ξ can be cast in the form[12]

$$\frac{d^2x}{d(k_p\xi)^2} = \frac{1}{2}\frac{1}{x^2} - 1 + \frac{2n_b}{n_0}] \tag{3.5}$$

where $x = \sqrt{(1-\beta)/(1+\beta)}$. It should be noted that Eq. (3.5) is equivalent to

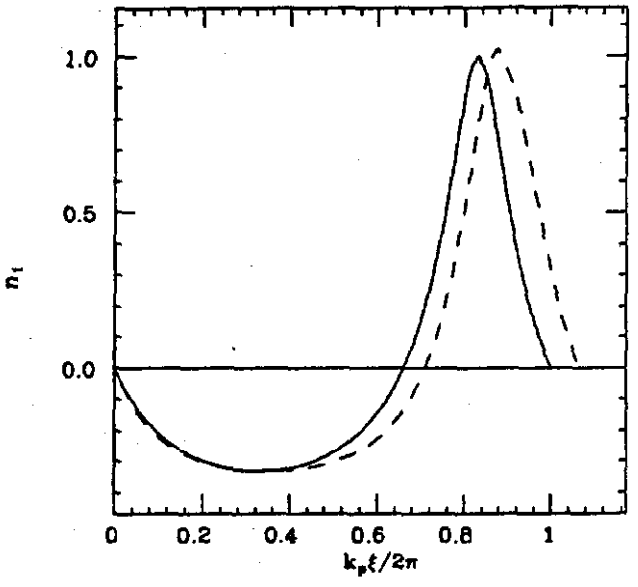

Figure 1. Perturbed plasma electron densities n_1/n_0 for one cycle of a nonlinear plasma wave, with maximum plasma fluid velocity $\beta_m = 0.5c$. The solid line represents the nonrelativistic solution; the dotted line shows the correct, period lengthened relativistic solution.

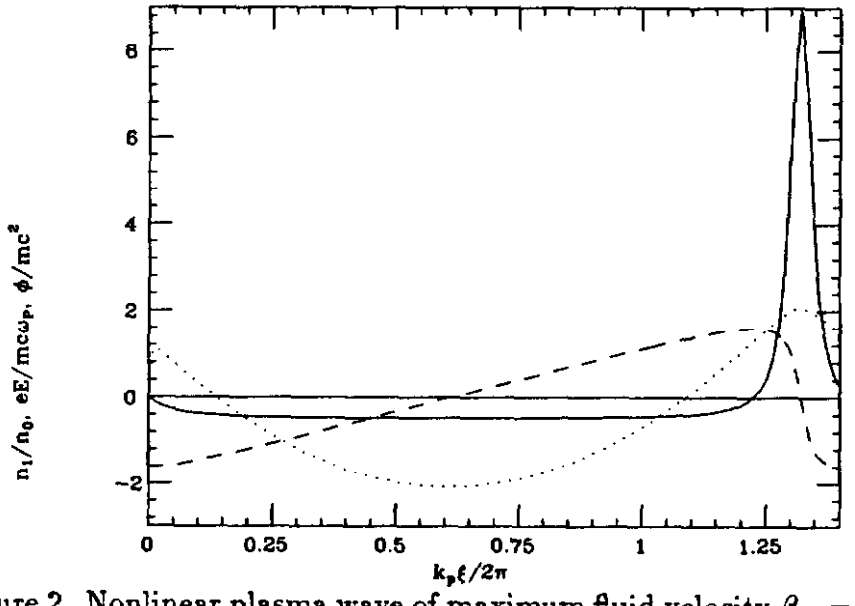

Figure 2. Nonlinear plasma wave of maximum fluid velocity $\beta_m = 0.9c$. Solid line shows n_1/n_0, dashed line indicates the electric force $-eE/m_e c\omega_p$, and dots represent the electrostatic potential $-e\phi/m_e c^2$.

the Poisson equation, as the electrostatic potential is given by $-\phi = m_e c^2 x$ and the perturbed electron density $n_1/n_0 = (x^{-2} - 1)/2$.

Some qualitative remarks on the solution to Eq. (3.5) are in order. The first is that the driven equation ($n_b > 0$) has a bifurcation between oscillatory and monotonically increasing behavior at $n_b = n_0/2$. This is in fact the required beam density for an enhanced transformer ratio in the proposed nonlinear PWFA scheme.[12] The undriven waves show oscillatory behavior, which in the large amplitude limit tends to exhibit long distances over which the perturbed plasma electron density approaches $-n_0/2$, interrupted by very narrow spikes of high positive density. The corresponding electric field becomes saw-toothed, with long linear rises followed by sharp drops, as illustrated in Fig. 2. The period expansion with amplitude physically comes from the relativistic mass increase of the plasma electrons; mathematically one can see that while for nearly linear waves ($|x - 1| \ll 1$) there is a linear restoring force in Eq. (3.5), for large amplitude waves where $x \gg 1$ the restoring force in the amplitude dependent oscillator saturates, forcing the local oscillation frequency down over much of the cycle and thus expanding the period. The expansion of the period allows for the possibility of electric fields larger than "wave-breaking".[14]

4. Nonlinear Plasma Wake-fields: Experiment

Much of the phenomena we have outlined above have been observed to some degree in the nonlinear PWFA experiments[6] at the AATF. We now examine a few of the most relevant observations from these experiments. The 21 MeV driving electron beam pulse used in the nonlinear experiments has the following characteristics: number of electrons per pulse $N = 2.5 \times 10^{10}$ ($Q = 4$ nC), rms pulse length $\sigma_z = 2.1$ mm, and initial rms radius $\sigma_r = 1.4$ mm. The plasma source length was set at $L_p = 33$ cm and plasma densities were variable between $n_0 = 0.5 - 8.0 \times 10^{13}$ cm^{-3}. The wake-fields in these experiments were directly measured by use of a low-intensity 15 MeV test electron bunch of similar dimensions to the

driving beam, which could be delayed to travel a variable distance behind the driver. The test beam could also be misaligned to measure transverse wake-fields. Both the energy spectrum and the transverse deflections of the test bunch were measured in a broad-range high resolution magnetic spectrometer. The data from these experiments is presented by taking the energy and transverse centroids of the test beam distribution a given time delay, and then stepping the delay sequentially with small time steps, repeating the centroid measurements at each time step. A plot of the test bunch energy or deflection centroid versus delay time is referred to as a wake-field scan.

To illustrate the most striking nonlinear PWFA phenomena observed we show two high resolution wake-field scans. The scan shown in Figs. 3-4, is taken with a relatively low plasma density $n_0 = 7.3 \times 10^{12}$ cm^{-3}. The witness and driver beams are horizontally misaligned in this scan to allow observation of the longitudinal dependence of the transverse wake-fields in this case. Several qualitative remarks can be made upon inspection of Figs. 3(a) and 4. The first is that both the longitudinal and transverse wake-fields are stable, oscillatory functions of the distance behind the driving beam ξ. In fact, the wake-fields suffer little degradation in form or amplitude out to 18 wavelengths behind the beam in this scan. This is surprising, as narrow nonlinear plasma wave may be subject to differences in frequency as a function of transverse position. Secondly, the longitudinal wake-fields W_z have taken on a more saw-tooth appearance, as we would be naively expect from the one-dimensional nonlinear theory. The transverse wake-fields show a form consistent with the Panofsky-Wenzel theorem, which implies that $W_z = \partial_z \int_0^r dr W_r$ for a cylindrically symmetric driver. It is apparent from inspection that the measured longitudinal wake-fields are to a good approximation proportional to the longitudinal derivative of the measured transverse wake-fields.

In addition to these qualitative remarks on the wave-forms, we have can examine the Fourier spectrum of the longitudinal wake-fields to attempt to quantify the physical basis for the nonlinearity of these waves using our perturbation treat-

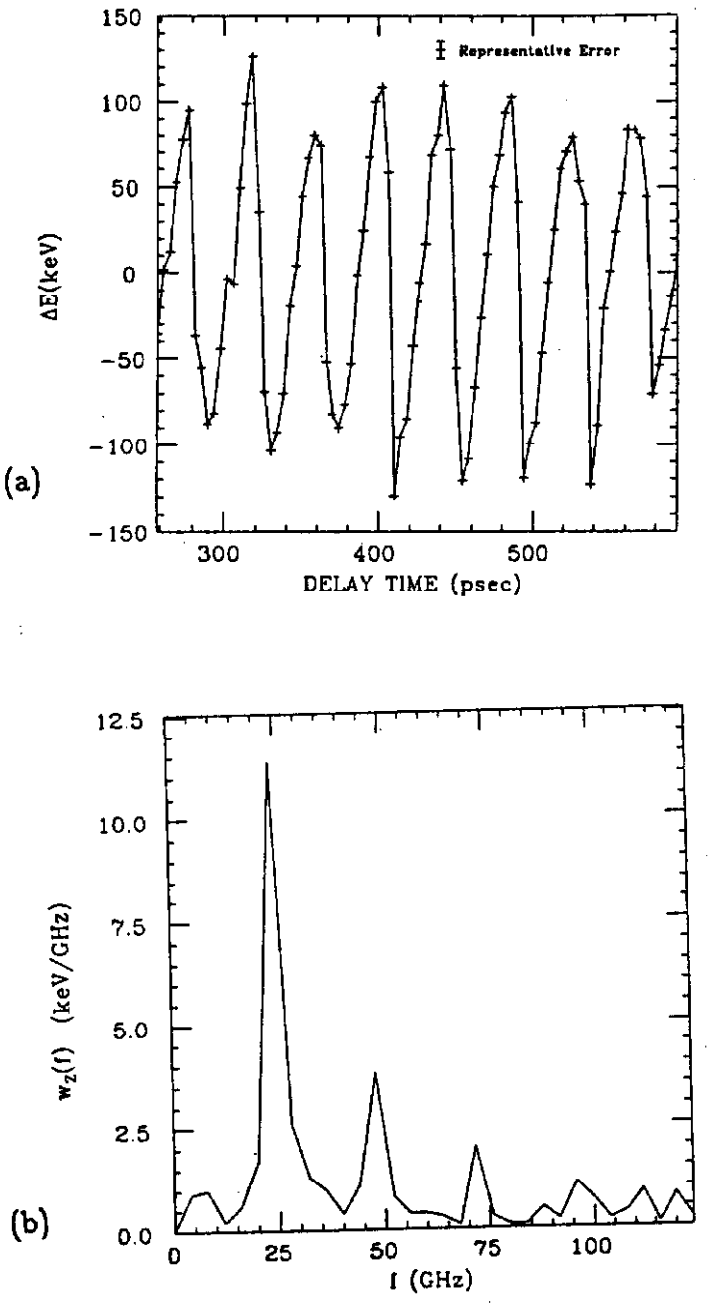

Figure 3. (a) Longitudinal wake-field scan – test beam energy centroid ΔE motion vs time delay, with plasma density of $n_0 = 7.3 \times 10^{12}$ cm^{-3}. (b) FFT amplitude function $w_z(f)$ for longitudinal wake-fields.

ment. The FFT of the longitudinal wake-field shown in Fig. 3(a) is displayed in Fig. 3(b); note that the ratio of first harmonic to the fundamental amplitude in the wake-fields is about 0.3. At a higher plasma density, which for the scan displayed in Fig. 5 is $n_0 = 2.8 \times 10^{13}$ cm^{-3} the longitudinal wake-fields display even more steepening. In this scan the the ratio of first harmonic E_2 to fundamental E_1 amplitude is 0.48. This wave amplitude is not consistent with the prediction excitation amplitude from linear theory if one ignores possible pinching of the driver beam. This is easily seen by using Eq. (3.4) to evaluate the the present case, with σ_r taken as its initial value to obtain $n_1/n_0 = 0.04$, which is much smaller than the estimate from harmonic content. This fact, along with other evidence available from the PWFA measurements,[6] led to the suggestion that significant self-pinching of the driver must have occurred, an assertion which was directly verified in later experiments.

The plasma skin-depth in the scan shown in Fig. 5 is 0.1 mm, or less than one-half of the rms beam length. This case is geometrically in the regime of the plasma lens. The dynamics and equilibration of the beam self-pinch will be explored in much greater detail below, so a simplified explanation of the the self-focusing effect on the nonlinear PWFA experiment is offered presently. Calculation using thick plasma lens theory[8] predict that the beam in this case will focus inside the plasma, and give an approximate equilibrium self-pinched beam radius is $\sigma_{eq} \simeq \epsilon\sqrt{\gamma/\nu}$, where ϵ is the beam transverse emittance, γ is the beam relativistic Lorentz factor and ν is Budker's parameter, the number of particles per unit length in units of a classical particle radius. The maximum current as a function of ξ in our beam corresponds to $\nu(0) = \nu_0 = 1.3 \times 10^{-2}$. Thus, with $\epsilon = 7 \times 10^{-6}$ m-rad we have $\sigma_{eq} = 0.44$ mm, or approximately one-third the original beam radius. This pinching is not uniform along the length of the beam, as in our model it depends on the enclosed current at a given point in ξ, a fact we can reflect by writing $\nu(\xi) = \nu_0 \exp(-\xi^2/2\sigma_z^2)$. We then have $\sigma_{eq}(\xi)^{-2} = (\nu_0\epsilon)\exp(-\xi/2\sigma_z^2)$., and the equilibrium density profile on axis is proportional to $\nu(\xi)/\sigma_{eq}^2 \sim \exp(-\xi/\sigma_z^2)$, *i.e.* the bunch is effectively shortened

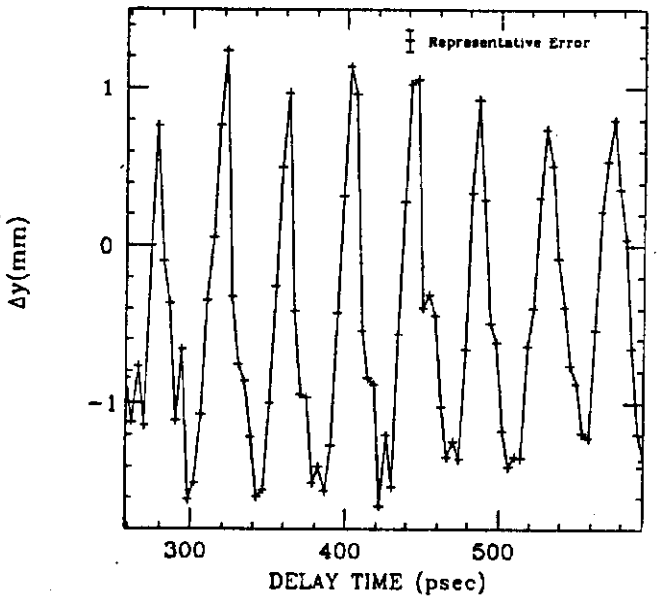

Figure 4. Transverse wake-field scan – test beam deflection plane centroid Δy vs time delay for the same scan as Fig. 3.

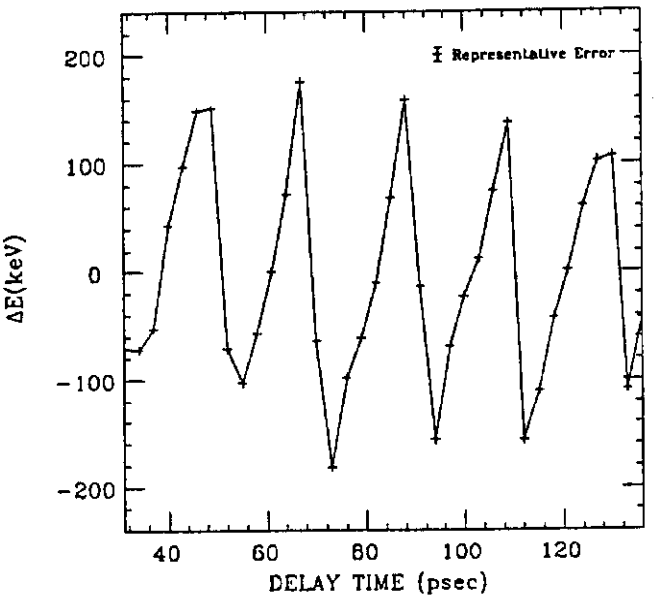

Figure 5. Longitudinal wake-field scan, with plasma of density $n_0 = 2.8 \times 10^{13}$ cm^{-3}.

on axis by a factor of $\sqrt{2}$. Both the beam pinching and the effective on axis pulse shortening serve to drive larger amplitude wake plasma waves, as can be seen from Eq. (3.4).

Taking into account the beam self-pinching the estimated ratio of the first harmonic to the fundamental in the second scan, using $\sigma_r = \sigma_{eq} = 0.44$ mm and $\sigma_z = 2.1/\sqrt{2}$ mm in the linear response formula, is $E_2/E_1 = 0.38$, in much better agreement with observation. If we apply the deconvolution analysis of Ref. 12 to include the effects of the finite resolution of the test beam, we obtain for this case a peak longitudinal field of $W_m = 5.3$ MeV/m. This is in reasonable accord with the value from Eq. (3.3) of 6 MeV/m, and with simulations performed at UCLA,[22] which indicate a maximum average accelerating gradient for this case of 7 MeV/m. The observed steepened form of the wake-fields is also reproduced well in the simulations. In regard to the maximum longitudinal field, it should be noted that no resolvable period lengthening has been observed in the PWFA experiments at the AATF, despite the large density nonlinearities. This is reflected in the fact that the wave-breaking field E_{wb} for this plasma density is over 500 MeV/m, and we have measured the field to only one percent of this value. In the one-dimensional limit E/E_{wb} is approximately the same as n_1/n_0. This does not occur in our case because the plasma electron motion becomes more radial due to the narrowness of the driving beam. This effect lowers the longitudinal field, and the plasma electrons do not attain relativistic velocities to support large density perturbations. Thus one would not expect period expansion in a narrow wave.

In these nonlinear PWFA measurements, the beam is narrower than a plasma skin-depth, and thus the plasma electron response and associated wake-fields cannot be well explained by a one-dimensional theory. Thus the theoretical arguments presented above should not be trusted to give quantitative predictions; we have been fortunate that the harmonic decomposition analysis agreed as well as it did with the measurements, and cannot expect this to be so in more nonlinear or narrower waves. A more rigorous approach to this problem would be desirable. Exact analysis remains an intractable problem; currently, perturbation

treatments of nonlinearities in relativistic phase velocity plasma waves are being developed by several investigators.[23] Particle-in-cell simulations have proven to be valuable so far in modelling nonlinear effects in the PWFA.[24] It is reasonable to suspect that simulations will continue to play an important role in understanding nonlinear plasma wake-fields. There are many questions that must still be addressed in this area, including the effect of multi-dimensional nonlinear effects on the transformer ratio in the PWFA, the stability of the nonlinear plasma oscillations – both in the one-dimensional limit and including transverse variations – and the maximum wake-field that can be expected in the limit that the beam is very narrow.

5. Nonlinear Beam Dynamics: Initial Self-Pinch

Much of the previous theoretical work on plasma wake-field focusing concerns the effect of a thin plasma lens on the transverse profile of a particle beam. In the present experiments, however, the plasma column is long compared to the focal length of the lens, and the beam dynamics are much more complex. In Ref. 8, there is a treatment of the problem of the thick lens correction to the thin lens which includes the effects of finite beam emittance and the raising of the focusing strength as the beam becomes more dense inside the lens. This analysis is not strictly applicable to the if the beam is not uniform in density, but shows interesting nonlinear characteristics. A phase-space distribution which allows use of this approach is the microcanonical distribution of Kapchinskii and Vladimirskii[25] (K-V distribution). In this distribution, in which the beam density is uniform out to the beam envelope, the emittance ϵ is defined to be four times the rms emittance, and equation for the beam envelope A can be written

$$A'' + \frac{2\nu}{\gamma A} = \frac{\epsilon^2}{A^3}, \tag{5.1}$$

where $'$ indicates a derivative with respect to z, The oscillations described by this equation are approximately simple harmonic if the envelope is not greatly

perturbed from its equilibrium value $A = \sqrt{\gamma/2\nu}\epsilon$. If the beam envelope is not closely matched to this value, then the solution to Eq. (5.1) predicts a large density spike ($n_b = \nu/\pi r_e A^2$) and period expansion with amplitude, as in the case of nonlinear plasma waves.

This coherent envelope motion does not exist for a non-K-V distribution, but is approximated only during the initial self-pinching for a beam which is initially larger than its equilibrium radius. In this case, the envelope dynamics can be simplified further by assuming laminar flow of the beam particles, an approach which is equivalent to setting $\epsilon = 0$ in Eq. (5.1) for a K-V beam. This approximation breaks down at the same point as the K-V treatment, as it also ignores the details of the self-consistent evolution of the beam phase space, but it allows us to simply estimate the distance to the first envelope minimum. Since the transverse wake-fields felt by a particle depend only on the enclosed current, which is conserved in laminar flow, and on the radius of the particle, each particle obeys an equation of motion for paraxial trajectories derivable from a logarithmic potential,

$$r'' + \frac{C(r_0)}{r} = 0, \tag{5.2}$$

where $C(r_0)$ is a constant dependent on initial radius r_0. Near the center of a cylindrical Gaussian this constant is given by $C(r_0) \simeq (\nu/\gamma)(r_0/\sigma_r)^2$, where γ is the Lorentz factor and we have introduced the Budker parameter ν, which is the number of particles per unit length measured in classical electron radii r_e. Integrating Eq. (5.2), the distance from the plasma boundary to the first focus is calculated,

$$s = \frac{1}{\sqrt{2C(r_0)}} \int_0^{r_0} \frac{dr}{\sqrt{\log(r_0/r)}} = r_0 \sqrt{\frac{\pi}{2C(r_0)}}. \tag{5.3}$$

This expression shows the linear dependence of this approximate half-oscillation period on initial amplitude. For a Gaussian initial profile one has $s \simeq \sigma_r \sqrt{\pi\gamma/\nu}$. In the AATF experiments where the transverse beam profiles are measured, described further below, the number of particles per bunch was $N = 3.2 \times 10^{10}$,

the rms bunch length $\sigma_z = 2.1$ mm and $\gamma = 42$, so the Budker parameter is $\nu = 1.6 \times 10^{-2}$. The beam is thus expected to come to its initial focus $s \simeq 8$ cm, which is well before the end of the plasma column of length $L = 35$ cm.

It is difficult to analytically estimate the minimum pinched beam radius in the presence of aberrations and finite initial emittance, because the transverse profile of the beam changes so dramatically as it focuses under the influence of nonlinear fields. The evolution of the rms beam envelope can be calculated by use of an equation which is formally identical to Eq. (5.1),[26] but in order to solve it one must known the evolution of the emittance, which is not a constant for non-K-V distributions. In order to solve for the emittance one must know the details of the phase space distribution. This subject can be addressed most straightforwardly by use of computer simulations. Computational treatments using a particle-in-cell code of this and related aspects of the self-pinching process will be presented below. Before proceeding to the computational work, an analytical model of the beam's approach to equilibrium is explored.

6. Nonlinear Beam Dynamics: Approach to Equilibrium

The transverse phase space dynamics of the beam under the influence of its self-focusing magnetic fields can be calculated in principle from the Maxwell-Vlasov equations, the self-consistent combination of the Maxwell electromagnetic field equations and the Vlasov equation, which is written

$$\frac{\partial f}{\partial t} + (\gamma m_e)^{-1} \mathbf{p}_\perp \cdot \nabla_{\mathbf{r}_\perp} f + \mathbf{F} \cdot \nabla_{\mathbf{p}_\perp} f = 0. \tag{6.1}$$

Here $f(\mathbf{r}_\perp, \mathbf{p}_\perp)$ is the beam's transverse distribution function and $\mathbf{F}$ is the Lorentz force arising from the charge and current distribution under consideration. In this case the force is due to the transverse wake-fields given by Eq. (2.7), which depend on the distribution of the beam particles in configuration space.

At this point it can be remarked that, because of the large nonlinearities in the radial focusing force and the effects of the individual particles' angular momentum, all particles have different effective betatron wave-numbers describing the periodicity of their orbits. Thus the initial coherent self-focusing motion of a set of particles decoheres as the particle motion becomes out of phase with each other, and the situation is approached where the distribution in configuration space becomes uncorrelated with the distribution in momentum space, *i.e.* the distribution seeks an equilibrium through collisionless or Landau damping. This approach to equilibrium through phase decoherence in the particle oscillations, whereby the coherent radial beam motion dissipates, was in fact initially sketched out by by Bennett in 1955, who termed the effect 'mixing'.[27] This effect is similar to a phenomenon, also referred to as decoherence, observed in the experimental study of nonlinear transverse dynamics in synchrotrons.[28] In our case, however, the nonlinear fields are provided by the beam distribution itself, and thus feedback is provided which allows us to view the dissipation of the coherent radial motion as a form of Landau damping.

As a specific type of stationary distribution is of present interest, the Maxwell-Vlasov equation is now written in cylindrincally symmetric equilibrium as

$$\frac{p_r}{\gamma m}\frac{\partial f}{\partial r} + W_r \frac{\partial f}{\partial p_r} = 0, \tag{6.2}$$

and the distribution function is assumed separable in coordinate and momentum dependence, $f(r, p_r) = R(r)P(p_r)$, because of the decorrelating effects of the nonlinearities. This assumption will be validated later by our computer simulations.

Upon substitution of the radial dependence of the magnetic self-force W_r from Eq. (2.7), and separation of variables, one obtains the momentum equation

$$\frac{\partial P}{\partial p_r} = -\frac{\alpha p_r}{\gamma m} P, \tag{6.3}$$

where $-\alpha$ is the separation constant, and the radial equation

$$\frac{\partial R}{\partial r} = -R\frac{2\alpha\epsilon^2\beta^2}{r}\int_0^r R(r')r'dr'. \tag{6.4}$$

The solution to the Eq. (6.3) is, of course, a Gaussian (thermal) distribution,

$$P = \sqrt{\frac{\alpha}{2\pi\gamma m}}\exp\left[-\alpha p_r^2/2\gamma m\right]. \tag{6.5}$$

The solution to the radial equation corresponding to this thermal equilibrium in momentum space is a Bennett profile[27] which has the form

$$R(r) \sim n_b(r) = \frac{\rho_b}{\left[1+(r/a)^2\right]^2} \quad , \tag{6.6}$$

where a is the Bennett radius. The usual expression for the Bennett radius relates it to the beam Debye length λ_D, with $\beta \simeq 1$,

$$a^2 = 8\lambda_D^2 = \frac{2kT_\perp}{\pi e^2\rho_b} = \frac{2kT_\perp}{\nu mc^2}a^2 \quad , \tag{6.7}$$

which only specifies the relationship between the beam transverse temperature and current, not the radius, which cancels out of the equation. This uncertainty can be be removed by invoking an approximate constraint on the asymptotic form of the distribution function.

To derive this constraint, note that from the form of the self-fields of a cylindrically symmetric beam and the associated Maxwell-Vlasov equation that the phase space density must be constant at $(\mathbf{r}_\perp, \mathbf{p}_\perp) = (\mathbf{0}, \mathbf{0})$, as from Eq. (6.1) we see that $\partial f/\partial t = 0$ there. If one takes an original four-dimensional phase space density corresponding to a cylindrically symmetric bi-Gaussian profile, and equates its initial value of $f(\mathbf{0},\mathbf{0})$ to the final value of $f(\mathbf{0},\mathbf{0})$ associated with the Bennett equilibrium, the Bennett radius is given by

$$a^2 = \frac{4\epsilon_n^2}{\gamma\nu}, \tag{6.8}$$

where $\epsilon_n = \beta\gamma\epsilon$ is the initial normalized emittance.

This argument is not strictly rigorous, however. Even though $f(\mathbf{0},\mathbf{0})$ is a constant of the motion, the form of the asymptotic state that we have assumed is not completely correct. It has been known for some time that the Bennett profile, being a state in thermal equilibrium, can evolve from a different initial state due to the thermalizing influence of multiple scattering of beam particles off the background plasma ions.[29] The distribution function can become smooth during this collisional process and thus approach the equilibrium solution to the Maxwell-Vlasov equation, which is the product of two smooth functions, a Bennett radial profile and Gaussian momentum profile.

In the case of the collisionless damping, however, the near-equilibrium state evolves from the initial pinch by filamentation of the beam phase space as it spirals under the influence of its own nonlinear self-fields. This filamentation process does not greatly affect the center of the distribution in phase space if the self-focusing forces there are nearly linear, which is the case for conditions not too far from equilibrium. This is because near equilibrium the small amplitude orbits in phase space are well behaved rotations about the fixed point of simple harmonic motion, $(\mathbf{0},\mathbf{0})$. On the other hand, large amplitude orbits experience very nonlinear fields, and the filamentation is quite pronounced in these regions of phase space. Since the derivation given above of the asymptotic Bennett radius is concerned with the final values of $f(\mathbf{r}_\perp,\mathbf{p}_\perp)$ at or near $(\mathbf{0},\mathbf{0})$, the fact that the motion near this point is well behaved makes the argument, which depends critically on approximation of the distribution as a smooth function at small amplitudes, quite accurate for cases relatively close too equilibrium.

If the motion is not well behaved even for small amplitude particles, as happens if the initial conditions are too far from equilibrium (*e.g.* $a \ll \sigma_r$), then the distribution function filaments near the origin in phase space, and the approximation of the actual distribution function as a product of smooth continuous functions is not as good. Filamentation at small amplitudes thus causes the asymptotic Bennett radius to be larger, and we rewrite Eq. (6.8) as an inequality, $a \geq 2\epsilon_n/\sqrt{\gamma\nu}$. In fact, other effects, such as a deviation from the assumed

initial cylindrical symmetry, spurious plasma oscillations or nontrivial return current density inside the beam radius will serve to strengthen this inequality. All of these effects are present in experiments to some extent.

As an aside, we note that the filamentation of phase space and associated emittance growth is closely related to the degree to which the beam is initially near its Debye shielded equilibrium. In the case of the magnetically self-constricted beam equilibrium, the Debye shielding length is essentially just the Bennett radius, as is seen from Eq. (6.7). The beam distribution is inherently thermal, and no fluid description is needed to describe the beam phase space. If the initial beam radius is much larger than the Bennett radius (Debye length), then the fluid motion of the beam is important, however, and filaments will form in phase space, effectively converting fluid motion into thermal motion. This behavior is also displayed in the related system of a space-charge dominated beam propagating in a constant focusing channel.[30-32] If a space-charge dominated beam is matched to a focusing in the rms sense, then the final emittance is given by[32]

$$\epsilon^2 = \epsilon_0^2 + \frac{K}{16} R^2 U_n \tag{6.9}$$

where R is the rms beam radius, K is the generalized beam perveance, and U_n is the normalized nonlinear field energy of the initial beam distribution, a dimensionless factor that is a measure of the degree of fluid motion in phase space necessary to shield the external focusing forces of the channel. As a space charge-dominated beam reconfigures to minimize its nonlinear field energy, it of course becomes more uniform, except for a region of a few Debye lengths near the beam edge where the density rapidly vanishes. It is seen from Eq. (6.9) that this process results in more phase space filamentation and emittance growth in the final state as the rms beam radius R becomes large compared to the Debye length $\lambda_D = (2K)^{-1/4}\sqrt{R\epsilon}$, or equivalently, as R is increased in comparison to the emittance. This corresponds to weaker focusing, or more laminar (fluid-like) initial flow of the beam. In this limit the spiralling beam fluid filaments in phase

space can occupy a region whose area is proportional to the rms beam radius, giving rise to the dependence seen in Eq. (6.9).

In the limit of applicable beam-plasma parameters, $k_p\sigma_z \gg 1 \gg k_p\sigma_r$, some predictions can now be made concerning the outcome of experiments. In the present experiments the normalized emittance $\epsilon_n = 3 \times 10^{-4}$ rad-m. Since the maximum in the beam current at $\xi = 0$ corresponds to a maximum Budker parameter of $\nu_0 = 1.6 \times 10^{-2}$, the minimum Bennett radius predicted from the Vlasov analysis is $a_0 \geq 0.72$ mm. This pinching is not uniform along the length of the beam, as in the model it depends on the current at a given point in ξ, a fact that can be reflected by writing $\nu(\xi) = \nu_0 \exp(-\xi^2/2\sigma_z^2)$. One then has $a(\xi)^{-2} = a_0^{-2} \exp(-\xi/2\sigma_z^2)$, and the equilibrium density profile on axis is proportional to $\exp(-\xi/\sigma_z^2)$, *i.e.* the bunch is effectively shortened on axis by a factor of $\sqrt{2}$.

7. Nonlinear Beam Dynamics: Simulation

In order to examine the deviations from the approximate theoretical treatments presented to this point, particle-in-cell simulations of the beam motion have been performed. In these calculations, which employed a modified version of the code EMMA,[33] written by Noble to calculate emittance growth in a space-charge dominated transport channel, cylindrical symmetry is assumed, longitudinal effects are ignored, and the wake-fields are calculated simply by using Eq. (2.7). The evolution of the beam distribution at one point in ξ can be quickly followed under these assumptions. Some relevant aspects of these computational results are presented here, which clarify the analytical work and provide more concrete predictions for the experimental data. These results are specialized in that the spurious effects of plasma oscillations are ignored in order to concentrate on the beam dynamics; fully electromagnetic $2\frac{1}{2}$-dimensional particle-in-cell simulations of beam self-focusing by plasma wake-fields have been performed previously.[11]

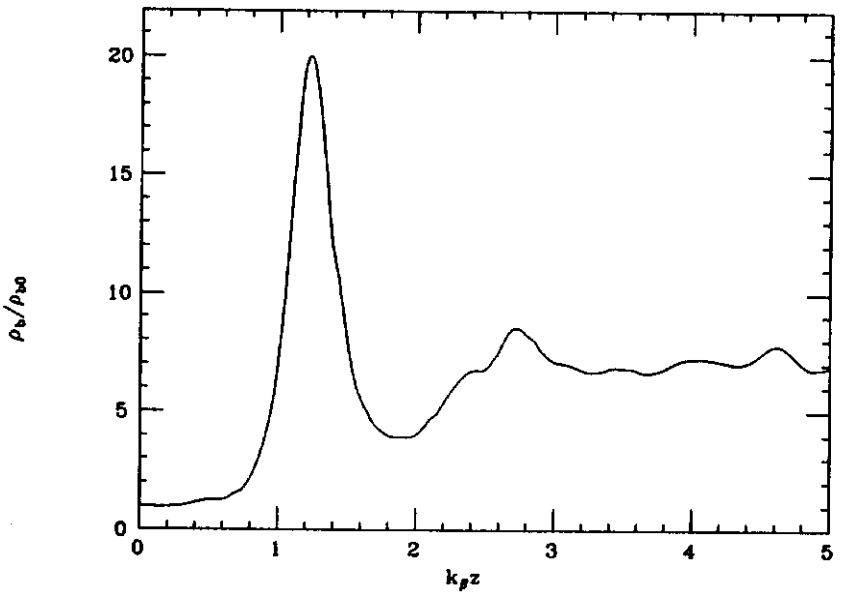

Figure 6. Peak calculated beam density ρ_b/ρ_{b0} as a function of $k_\beta z$, for initial condition $a/\sigma_r = 0.51$. For minimum equilibrium Bennett radius $\rho_b/\rho_{b0} = 7.85$.

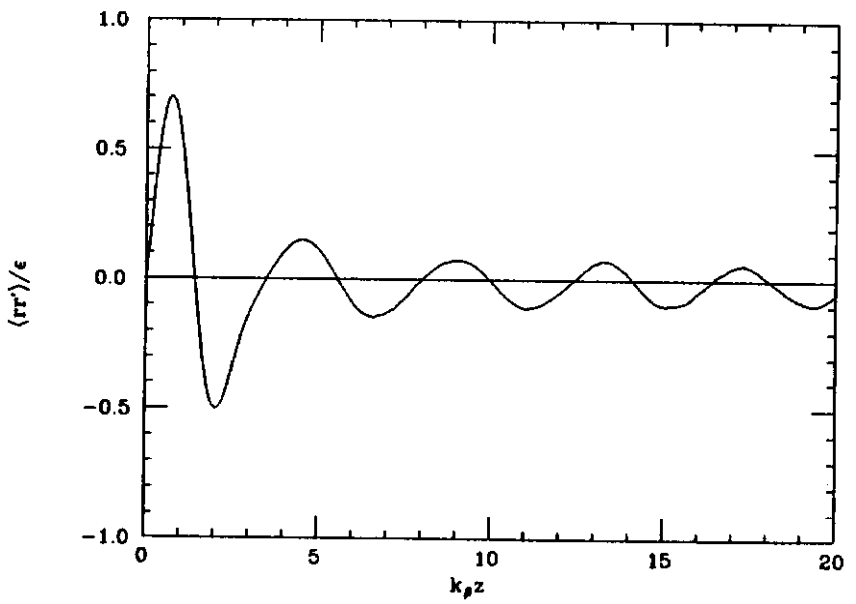

Figure 7. Calculated correlation parameter $\langle rr' \rangle / \epsilon_r$ as a function of $k_\beta z$, for initial condition $a/\sigma_r = 0.51$.

To begin, we examine the evolution of the peak beam density ρ_b/ρ_{b0} as it self-pinches, which is shown in Fig. 6. The longitudinal distances are given in units of k_β^{-1}, where $k_\beta = \sqrt{\nu/\gamma\sigma_r^2}$ is the initial small amplitude betatron wavenumber in the beam's self-focusing wake-field. All parameters in the computations shown correspond to the strongest focusing experimental case, in which $a/\sigma_r = 0.51$, where the initial beam distribution function is Gaussian in momentum and co-ordinate and the beam is at a waist. The initial pinching occurs in $k_\beta s = 1.27$, which is in excellent agreement with the value of $k_\beta s = \sqrt{\pi/2} \simeq 1.25$ derived in Eq. (5.3). The peak beam density is approximately 20 times the initial peak density at this point; after slight defocusing, it subsequently does not reach such large densities, but tends rapidly towards equilibrium. The maximum predicted equilibrium density associated with $a/\sigma_r = 0.51$ is $\rho_b/\rho_{b0} = 2(\sigma_r/a)^2 = 7.85$. It appears that the equilibrium which develops is slightly less dense than this.

The fluctuations in the peak density have nearly damped after $k_\beta z = 3$, or one beam envelope oscillation, which is extremely quick. The degree to which the distribution function comes into equilibrium, *i.e.* approaches a separable Bennett-coordinate/Gaussian-momentum form, can be quantified by examining the correlation parameter $\langle rr' \rangle / \epsilon_r$. Here $\epsilon_r = \sqrt{\langle r^2 \rangle \langle (r')^2 \rangle - \langle rr' \rangle^2}$ is the radial rms emittance. The evolution of this parameter is shown in Fig. 7. After initial large excursions associated with the first focus and defocus, the correlations then damp more slowly while oscillating with period $k_\beta \lambda \simeq 4$. These oscillations do not in large part reflect oscillation of the core of the beam, as these would have a period $k_\beta \lambda = 2\pi(a/\sigma_r) \simeq 3.2$, and would show up also in Fig. 6. The correlations are instead due to the spiralling 'arms' of the distribution, which occur at large amplitude and thus have a lower average wave-number. These spirals, which come into equilibrium more slowly than the beam core due to the decrease in focusing strength with amplitude and the larger initially empty regions of phase space with which they must mix, have been observed in the simulations; they are not shown in the interests of brevity. These results support the conclusion that the phase space correlations in the beam core indeed dissipate quickly, after one

radial oscillation, as is necessary to apply the results of the Vlasov analysis.

It is apparent from Fig. 6 that the maximum beam density has stabilized by $k_\beta z = 5$, which corresponds to the length of the plasma column in these experiments. It is reassuring to plot the transverse profile of the beam density at this point, as is shown in Fig. 8, along with the Bennett profile from the theoretical prediction of the Vlasov treatment. The calculated profile is slightly less dense and has a marginally wider core than the minimum-radius Bennett profile, indicating small effects due to phase space filamentation.

Thus the simulations confirm the major conclusions of the analytical approaches that have been developed, and give additional insight into the expected experimental results. The observation of core equilibration within $k_\beta z = 3$ allows use of the results of the Vlasov treatment to predict the self-pinched beam radius, as this equilibration length is shorter than the plasma column in the measurements, which are presently described.

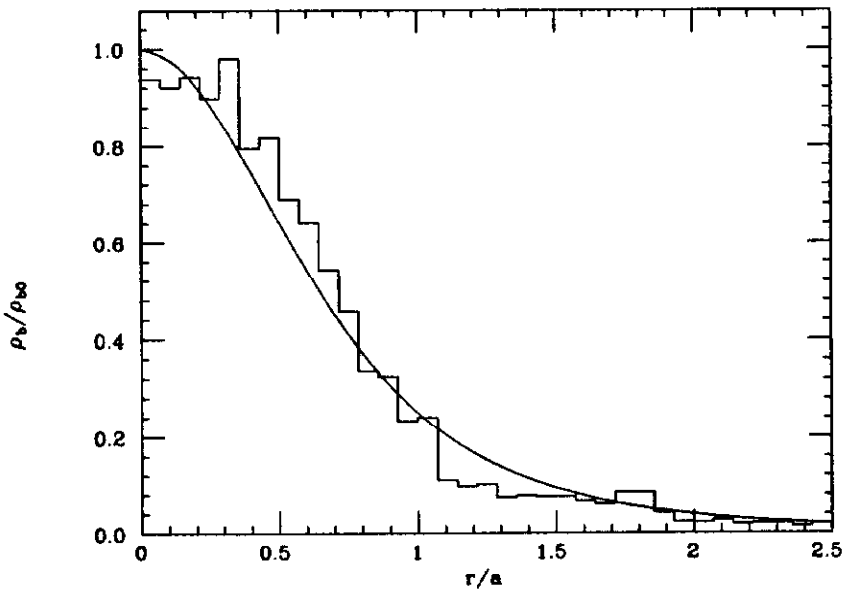

Figure 8. Histogram of the calculated beam density at $k_\beta z = 5$ (the end of the plasma column in the experiments), for initial condition $a/\sigma_r = 0.51$. Solid line is the Bennett profile predict by the Vlasov treatment.

8. Measurement of Self-focused Beam Profiles in Plasma

In order to further investigate the mechanisms behind the wake-field excitation of nonlinear plasma waves and to test aspects of plasma focusing theory, experimental measurements of the self-focused beam profiles at the end of a plasma column have been recently performed at the AATF.[34] The beam pulse delivered to the plasma source has, to restate, the following parameters; $N \simeq 3.2 \times 10^{10}$ electrons, rms length $\sigma_z \simeq 2.1$ mm transverse emittance $\epsilon \simeq 7 \times 10^{-6}$ m-rad, and $\sigma_r \simeq 1.4$ mm. This experiment used a one-picosecond resolution streak camera as the basis of a diagnostic that allowed measurement of the transverse profile of the beam as a function of longitudinal position in the beam. We summarize the results of these measurements here; for a detailed discussion see Ref. 34.

The time resolved pictures of the beam intensity profile obtained in this manner confirmed that at high plasma density ($k_p\sigma_z \geq 2$), the beam profile was self-pinched with equilibrium radius dependent on ξ, with the narrowest profile occurring at the current maximum, as expected. This self-pinched distribution led to effective pulse shortening on axis, also validating a theoretical prediction. As an example of a self-pinched profile we will show a case where the plasma density $n_0 = 6.0 \times 10^{13}$ cm^{-3}. In terms of the initial beam profile, this corresponds to a beam length in plasma radians $k_p\sigma_z \simeq 3$, and is thus inside the regime where the plasma space charge neutralizes the beam and magnetic self-focusing occurs.

The plots in Fig. 9 shows the transverse cross-section (a projection of the most intense 0.5 mm long transverse strip) of the beam intensity streak image for the dense plasma present and absent. In the case of plasma absent shown in Fig. 9(b), we also include a best fit of the data, to a Gaussian of width $\sigma_r = 1.4$ mm, with a dashed line. When the dense plasma is present the self-pinched profile shown in Fig. 9(a) is obtained, with a best fit of the data, to a Bennett profile of radius $a = 0.91$ mm, indicated by the dashed line. The agreement in form is about as good as would be expected on the basis of the profile shown in Fig. 8. Recall that the minimum predicted Bennett radius for this case is $a_0 = 0.72$

mm. The experimentally measured value is larger by about 25% due to the effects previously mentioned; the beam does not have perfect cylindrical symmetry initially, and deviations from this ideal undoubtedly allow more filamentation and effective dilution of the phase space density of the beam. In addition, there are effects due to the plasma response; even in the high plasma density case considered here the product $k_p\sigma_z$ which results on axis after pinching (due to the effective pulse shortening described above) is about 2.2, which is just on the border of the adiabatic regime of the plasma electron fluid motion where one can assume approximate charge neutralization of the beam. The focusing in the core of the beam can be lowered by the lag of the plasma electron response to the larger gradients in the beam charge density.

The effects of this response lag are displayed in Fig. 10. The on-axis beam profiles – projection of the most intense 0.2 mm wide longitudinal strip – of the beam image are plotted for four different plasma densities, $n_0 = 0.9, 1.5, 2.9,$ and 6.0×10^{13} cm^{-3} (dashed, dotted, dot-dash and solid lines, respectively). At low density the plasma skin-depth is longer than the beam scale length and the maximum focusing, reflected by the maximum in beam intensity, lags the current maximum. At the highest plasma density, the plasma response is nearly adiabatic and the on-axis profile regains its symmetric, Gaussian-like shape. The rms beam length for the highest density case is $\sigma_z = 1.5 \simeq 2.1/\sqrt{2}$ mm, in agreement with our naive prediction concerning the on-axis pulse shortening. This observation is important, as it is necessary to invoke pulse shortening to attempt explanation of the wake-field nonlinearity observed in Fig. 5. More detailed presentation and discussion of the results of the plasma wake-field focusing experiments at the AATF can be found in Ref. 34.

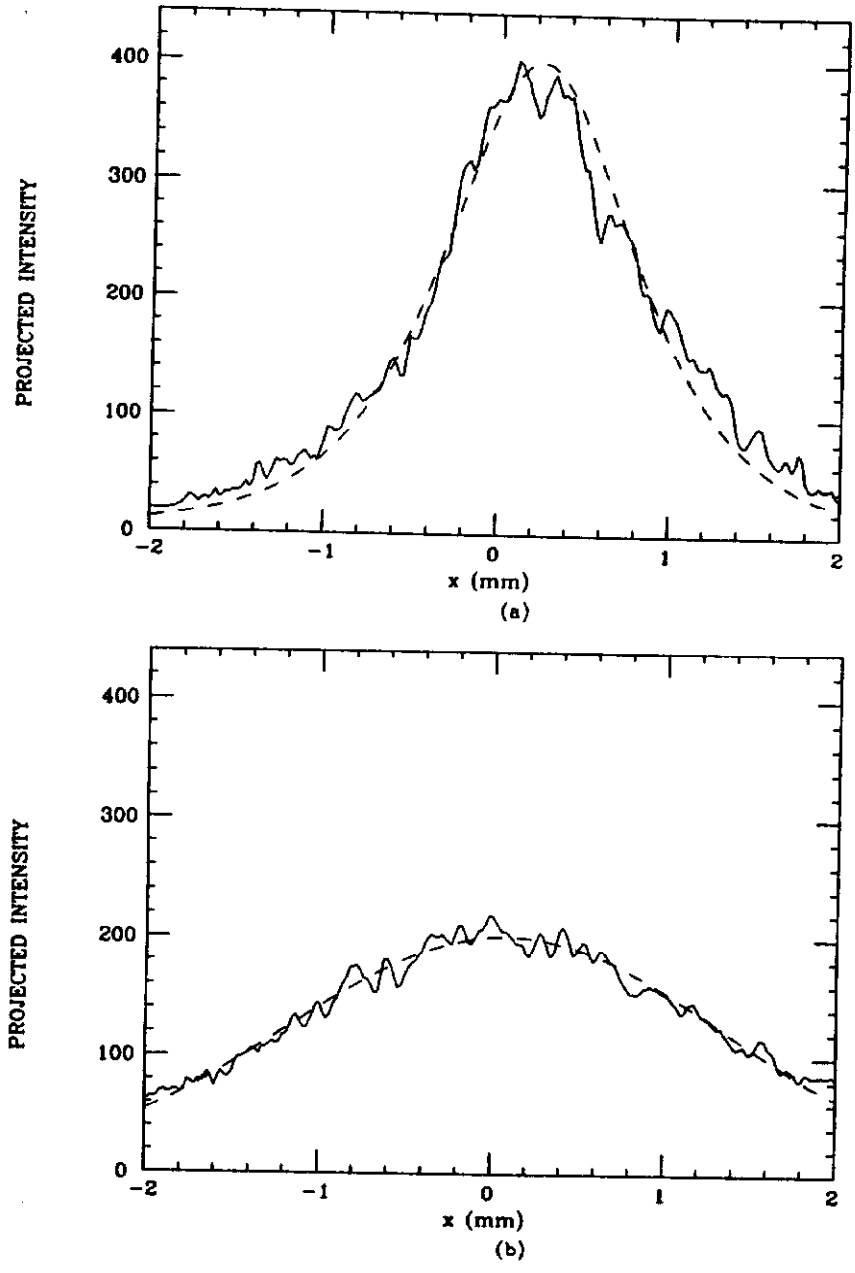

Figure 9. Plots of beam transverse intensity profiles (a projection of the most intense 0.5 mm long transverse strip in the streak image) (a) With dense plasma present – the self-pinched profile (solid line) with a best fit of the data to a Bennett profile of radius $a = 0.91$ mm (dashed line). (b) With no plasma – the unpinched profile (solid line) with a best fit of the data to a Gaussian profile of width $\sigma_r = 1.4$ mm (dashed line).

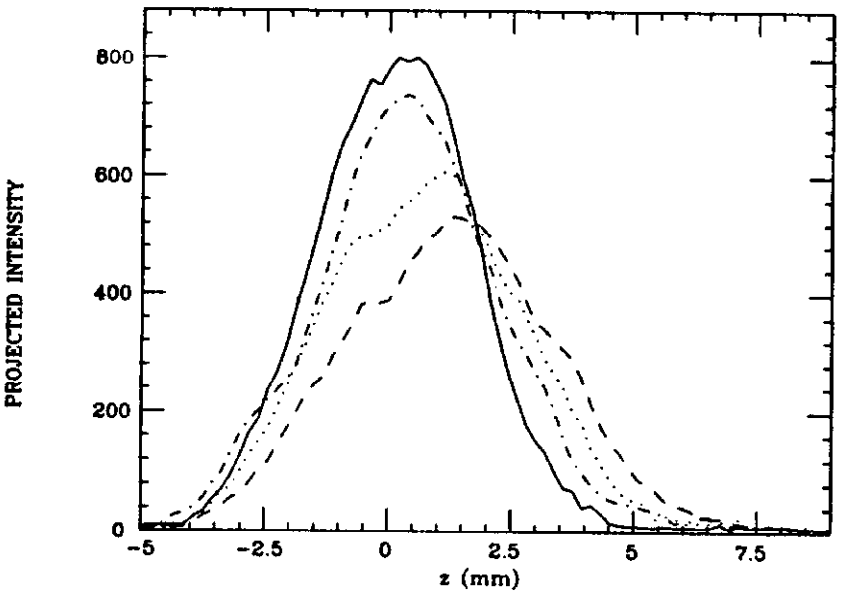

Figure 10. The on-axis beam profiles – projection of the most intense 0.2 mm wide longitudinal strip – of the beam image, plotted for four different plasma densities, $n_0 = 0.9, 1.5, 2.9$, and 6.0×10^{13} cm^{-3} (dashed, dotted, dot-dash and solid lines, respectively).

9. Conclusions

In this paper we have examined experimental and theoretical aspects of nonlinear beam and plasma physics in plasma wake-fields. The beam and plasma behavior are, of course, intimately related experimentally, and this presentation has partially been an attempt to reflect that relationship. As a whole, the theoretical picture we have drawn explains the experimental situations encountered quite well. The experimental results to form a fairly self-consistent and nearly complete set, in that they investigated the obvious physical questions in beam and plasma parameters accessible with present experimental facilities.

Having understood past and present experiments with their challenging nonlinear attributes to a fair degree of satisfaction, we can look with some trepidation and excitement towards the future. The planned upgrade of the AATF[35] at Argonne will include a 150 MeV low emittance electron beam, with 100 nC in 5 psec pulse. The peak current in this beam is 75 times that used in the present nonlinear wake-field experiments. With this beam one can access a regime where the beam will actually be denser than the plasma ($n_0 \sim 2 \times 10^{14}$ cm^{-1}). None of the approximations we have used to explain the plasma response will be of reasonable validity in this limit. While the plasma physics in this regime becomes much more nonlinear, the transverse beam behavior becomes more linear – inside the beam the plasma electrons will be completely ejected, leaving a uniform density ion column which gives rise to linear focusing forces. This is the regime of the underdense plasma lens,[10,11] which is superior to the overdense case we have considered as a final focusing linear-collider lens. This is due to the background problem that can arise from the hard beam lepton-plasma ion collisions. Demonstration of underdense plasma focusing is one interesting result that may arise from future AATF experiments. Depending on the details of the plasma response, one can also conceive of observing accelerating gradients in these nonlinear wake-fields which are approximately "wave breaking" amplitude, which is greater than 1 GeV/m for projected plasma densities. More computa-

tional investigation of these experimental scenarios is necessary to obtain more rigorous predictions concerning the nonlinear wake-fields driven by very intense electron beams. At the same time, it would also be most beneficial to have useful analytical models of the three-dimensional nonlinear plasma response, in order to better understand the fundamental physics of the plasma wake-field interaction.

REFERENCES

1. P. Chen, J. M. Dawson, R. W. Huff, and T. Katsouleas, *Phys. Rev. Lett.*, **54,** 693 (1985).
2. T. Katsoulcas, *Phys. Rev. A* **33,** 2056 (1986).
3. R. D. Ruth, A. Chao, P. L. Morton, and P. B. Wilson, *Particle Accelerators* **17,** 171 (1985) .
4. R. Keinigs and M. Jones, *Physics of Fluids* **30,** 252 (1987).
5. J. B. Rosenzweig, D. B. Cline, B. Cole, H. Figueroa, W. Gai, R. Konecny, J. Norem, P. Schoessow, and J. Simpson, *Phys. Rev. Lett.* **61,** 98 (1988).
6. J. B. Rosenzweig, P. Schoessow, B. Cole, W. Gai, R. Konecny, J. Norem and J. Simpson, *Phys. Rev. A – Rapid Comm.*, **39,** 1586 (1989).
7. P. Chen, *Particle Accelerators* **20** (1985) 171.
8. J. B. Rosenzweig and P. Chen, *Phys. Rev. D* **39,** 2039 (1989).
9. J. B. Rosenzweig, B. Cole, D. B. Cline, and D. J. Larson, *Particle Accelerators*, **24,** 11 (1988).
10. P. Chen, S. Rajagoplan, and J. B. Rosenzweig, *Phys. Rev. D* **40,** 923 (1989).
11. J.J. Su, T. Katsouleas, J. Dawson and R. Fedele, UCLA Report PPG-1177, 1988, submitted to *Phys. Rev. A.*
12. J. B. Rosenzweig, *Phys. Rev. Letters*, **58** (1987) 555.
13. R.J. Noble, *Proceedings of the Twelfth International Conference on High Energy Accelerators*, (Fermilab, Batavia, IL, 1984)
14. J. B. Rosenzweig, *Phys. Rev. A*, **38,** 3634 (1988).
15. T. Katsouleas and W. B. Mori, *Phys. Rev. Lett.*, **61,** 90 (1988).
16. A.Ts. Amatuni, S.S. Sekhpossian and E.V. Elbakian, Yerevan Preprint YerPhi-935(86)-86 Yerevan, USSR (1986).

17. J. B. Rosenzweig, *Phys. Rev. A*, **40,** 5249 (1989).

18. W.K.H. Panofsky and W.A. Wenzel, *Ref. Sci. Instrum.* **27,** 967 (1956).

19. B. Autin, A.M. Sessler and D.H. Whittum, *Proceedings of the 1989 IEEE Particle Accelerator Conference*, 1812 (IEEE, New York, 1989).

20. D. Umstadter, R. Williams, C. Clayton, and C. Joshi, *Phys. Rev. Lett.* **59,** 292 (1988).

21. J.M. Dawson, *Phys. Rev.* **113,** 383 (1959).

22. J.J. Su, presented at the Lake Arrowhead Workshop on Advanced Accelerator Concepts (Lake Arrowhead, CA 1989).

23. W.B. Mori, J.J. Su, and G. Miano, private communication.

24. J.J. Su, T. Katsouleas, J. Dawson, P. Chen, M. Jones and R. Keinigs, *IEEE Trans. Plasma Sci.* **PS-15,**192 (1987).

25. I.M. Kapchinskii and V.V. Vladimirskii, *Proc. of International Conference on High Current Accelerators*, 274 (CERN, Geneva, 1959)

26. F. Sacherer, *IEEE Trans. Nucl. Sci.* **18,** 1105 (1971).

27. W. H. Bennett, *Phys. Rev.* **45,** 890 (1934), and *Phys. Rev.* **98,** 1584 (1955).

28. A. Chao, D. Johnson, S. Peggs, J. Peterson, C. Saltmarsh, L. Sachinger, R. Meller, R. Siemann, R. Talman, D. Edwards, D. Finley, R. Gerig, N. Gelfand, M. Harrison, R. Johnson, N. Merminga, and M. Syphers, *Phys. Rev. Lett.* **61,** 2752 (1988).

29. E.P. Lee, *Phys. Fluids* **19,** 60 (1976).

30. T.P. Wangler, K.R. Crandall, R.S. Mills and M. Reiser, *IEEE Trans. Nucl. Sci.* **32,** 2196 (1985).

31. J. Struckmeier, J. Klabunde and M. Reiser, *Particle Accelerators* **15,** 47 (1984).

32. O.A. Anderson, *Particle Accelerators* **21,** 197 (1987).

33. R. J. Noble, *Proceedings of the 1989 Particle Accelcrator Conference,* 1067 (IEEE, New York, 1989).

34. J. B. Rosenzweig, W. Gai, C.H. Ho, R. Konecny, S. Mtingwa, J. Norem, M. Rosing, P. Schoessow and J. Simpson, accepted for publication in *Phys. Flu. B.*

35. W. Gai, C. Ho, R. Konecny, S. Mtingwa, J. Norem, J. Rosenzweig, J. Simpson, B. Cole and M. Rosing, *Proceedings of the 1989 Particle Accelerator Conference,* 612 (IEEE, New York, 1989).